1-1-2014

Electrophysiological Phenotypes Of Mecp2 A140V Mutant Mouse Model

Lu Yao Ma

Chen Wu

Yu Jin

Ming Gao

Guo Hui Li

See next page for additional authors

Authors

Lu Yao Ma, Chen Wu, Yu Jin, Ming Gao, Guo Hui Li, Dharshaun Turner, Jian Xin Shen, Shi Jiang Zhang, Vinodh Narayanan, Garilyn Jentarra, and Jie Wu

CNS Neuroscience & Therapeutics

ORIGINAL ARTICLE

CNS Neuroscience & Therapeutics

Electrophysiological Phenotypes of MeCP2 A140V Mutant Mouse Model

Lu-Yao Ma,[1,2] Chen Wu,[1] Yu Jin,[1] Ming Gao,[1] Guo-Hui Li,[1] Dharshaun Turner,[1] Jian-Xin Shen,[3] Shi-Jiang Zhang,[2] Vinodh Narayanan,[4] Garilyn Jentarra[4,5] & Jie Wu[1,3]

1 Division of Neurology, Barrow Neurological Institute, St. Joseph's Hospital and Medical Center, Phoenix, AZ, USA
2 Department of Cardiothoracic Surgery, The First Affiliated Hospital with Nanjing Medical University, Nanjing, China
3 Department of Physiology, Shantou University Medical College, Shantou, China
4 Pediatric Neurology Department, Barrow Neurological Institute, St. Joseph's Hospital and Medical Center, Phoenix, AZ, USA
5 Department of Biochemistry, Midwestern University, Glendale, AZ, USA

Keywords
Electrophysiology; Hippocampal slice; Long-term potentiation; MeCP2 gene; Rett model; Synaptic transmission.

Correspondence
J. Wu, M.D., Ph.D., Division of Neurology, Neurophysiology Laboratory, Barrow Neurological Institute, St. Joseph's Hospital and Medical Center, 350 West Thomas Road, Phoenix, AZ 85013-4496, USA.
Tel.: +(602)-406-6376;
Fax: +(602)-406-7172;
E-mail: jie.wu@dignityhealth.org
or
G. Jentarra, Ph.D., Department of Biochemistry, Midwestern University, 19555 N 59th Ave, Glendale, AZ 85308, USA.
Tel.: +(623)-572-3334;
Fax: +(623)-572-3679;
E-mail: gjenta@midwestern.edu
Received 19 July 2013; revision 27 December 2013; accepted 3 January 2014

SUMMARY

Aims: MeCP2 gene mutations are associated with Rett syndrome and X-linked mental retardation (XLMR), diseases characterized by abnormal brain development and function. Recently, we created a novel MeCP2 A140V mutation mouse model that exhibited abnormalities of cell packing density and dendritic branching consistent with that seen in Rett syndrome patients as well as other MeCP2 mutant mouse models. Therefore, we hypothesized that some deficits of neuronal and synaptic functions might also be present in the A140V mutant model. **Methods:** Here, we tested our hypothesis in hippocampal slices using electrophysiological recordings. **Results:** We found that in young A140V mutant mice (3- to 4-week-old), hippocampal CA1 pyramidal neurons exhibited more positive resting membrane potential, increased action potential (AP) firing frequency induced by injection of depolarizing current, wider AP duration, and smaller after hyperpolarization potential compared to neurons prepared from age-matched wild-type mice, suggesting a neuronal hyperexcitation. At the synaptic level, A140V mutant neurons exhibited a reduced frequency of spontaneous IPSCs (inhibitory postsynaptic potentials) and an enhanced probability of evoked glutamate release, both suggesting neuronal hyperexcitation. However, hippocampal CA1 long-term potentiation was not significantly different between A140V and WT mice. In adult mice (11- to 13-month-old), in addition to neuronal hyperexcitation, we also found significant deficits of both short-term and long-term potentiation of CA3-CA1 synapses in A140V mice compared to WT mice. **Conclusions:** These results clearly illustrate the age-dependent abnormalities of neuronal and synaptic function in the MeCP2 A140V mutant mouse model, which provides new insights into the understanding of the pathogenesis of Rett syndrome.

doi: 10.1111/cns.12229

The first two authors contributed equally to this work.

Introduction

The MeCP2 gene encodes the methyl CpG DNA binding protein 2. MeCP2 has been described as both an activator and a repressor of transcription and functions in complex with a variety of proteins to bind the regulatory regions of genes and affect their transcription [1–3]. Reports also suggest that MeCP2 may be directly involved in modifying gene expression through chromatin remodeling activities rather than direct binding to specific gene promoters [4–7]. The most prominent disorder associated with MeCP2 mutations is Rett syndrome (RTT; OMIM 312750), an X-linked neurodevelopmental disorder [8].

Classic RTT is characterized by relatively normal development for the first 6–18 months of life followed by a period of regression involving the loss of acquired skills such as speech and voluntary hand movements. Males with MeCP2 mutations often have severe neonatal encephalopathy and die at 1–2 years of age. Thus, the majority of RTT patients are female. Symptoms of RTT include cognitive and motor abnormalities, microcephaly, stereotyped movements, autistic features, and seizures [9–14].

The pathological features found in the brains of RTT patients include small brain size, increased brain cell packing density, and abnormalities of neuronal dendrites and dendritic spines, which has been particularly noted in the pyramidal neurons of the cortex [9,15–18]. Gene duplications of MeCP2 are also pathogenic and can be just as deleterious as mutations in the gene, indicating that gene dosage of MeCP2 is critical to proper neuronal function [19].

While MeCP2 mutations are often catastrophic in males, there are reports of surviving males with MeCP2 mutations [14,20]. The A140V point mutation is one of the few MeCP2 mutations that is survivable long term in males and results in an X-linked mental retardation syndrome (XLMR) rather than classic Rett syndrome. XLMR due to the A140V mutation is described primarily in males as they suffer the most serious symptoms. Females carrying this mutation are either unaffected or suffer mild mental retardation. Symptoms of MECP2 A140V XLMR include mental retardation, mild microcephaly, motor abnormalities, PPM-X syndrome, and dysarthric speech [21–25]. We have previously described our construction and characterization of the MeCP2 A140V mouse model. In this model, we identified brain pathology consistent with that seen in RTT patients and in other MeCP2 mutant mouse models, including increased cell packing density and a marked decrease in the dendritic branching of cortical pyramidal neurons [26].

Several electrophysiology studies have been performed on brain tissue from RTT mouse models. These studies have led to the identification of impairments of synaptic plasticity in brain regions including the cortex [27–30], hippocampus [30–33], thalamus [34], and various brain stem structures [35,36]. Tests on MeCP2-null mouse models revealed that symptomatic mice have deficits of hippocampal long-term potentiation (LTP) as well as long-term depression (LTD). Deficits of short-term plasticity were identified using a paired-pulse facilitation method (PPF) [31]. A RTT mouse model with a C-terminal truncation of the MeCP2 gene (308/y) has also undergone electrophysiological testing. This testing identified abnormalities of LTP and LTD in hippocampal tissue, similar to that seen in the MeCP2 null mice, and demonstrated enhanced synaptic transmission by input/output analysis. PPF was impaired in the 308/y mice, again implying an enhancement of synaptic transmission through increased neurotransmitter release. This group also found LTP deficits in the layer II/III primary motor and sensory cortex neurons [30]. An additional study of layer 5 in the cortical pyramidal neurons in a MeCP2 null model failed to identify LTP deficits but found reduced excitatory synaptic connectivity [28].

Here, we report the results of electrophysiological studies of hippocampal CA1 pyramidal neurons from the MeCP2 A140V mutant mouse model. We have identified abnormalities of neuronal firing, basal synaptic function, and neuronal excitability as well as deficits of both short-term and long-term potentiation of CA3-CA1 synapses in the mutant mice. These abnormalities correlate well with previous reports regarding the electrophysiological dysfunction of neurons from other MeCP2 mutant mouse models.

Materials and methods

Experimental Animals

Heterozygous MeCP2 A140V females produced in our colony were bred with wild-type male C57BL/6 mice to produce the male MeCP2 A140V hemizygous mice used in these experiments. All breeding and experimentation were conducted in accordance with IACUC-approved protocols.

Hippocampal Slice Preparation

Hippocampal Slice Preparation from Young Mice and Patch-Clamp Recordings

Several coronal hippocampal slices (250 μm) were prepared from young (20- to 30-day-old) mice including wild-type and A140V mutant mice. Slices were cut using a vibratome (Vibratome 1000 Plus, St. Louis, MO, USA) in ice-cold glycerol-based artificial cerebrospinal fluid (GACSF) containing (in mM): 250 Glycerol, 2.5 KCl, 1.2 NaH_2PO_4, 1.2 $MgCl_2$, 2.4 $CaCl_2$, 26 $NaHCO_3$, and 11 glucose [37]. The slices were then allowed to recover for at least 1 h in a holding chamber at room temperature (21–22°C) in normal incubation solution containing (in mM): 125 NaCl, 3 KCl, 2 $CaCl_2$, 1 $MgCl_2$, 1.25 NaH_2PO_4, 26 $NaHCO_3$, and 10 glucose continuously saturated with 95% O_2 and 5% CO_2.

Hippocampal Slice Preparation from Adult Mice and Field Potential Recordings

Hippocampal slices were prepared from mice that were 11- to 13-month-old (WT and A140V) mice. Brains were rapidly removed under deep isoflurane anesthesia and bathed in cold (4°C) artificial cerebrospinal fluid (ACSF) containing (in mM): NaCl 119; KCl 2.5; $NaHCO_3$ 26; $MgSO_2$ 1.3; NaH_2PO_4 1.0; $CaCl_2$ 2.5 and glucose 11; pH 7.4. The ACSF was continuously bubbled with 95% O_2–5% CO_2 (carbogen). Coronal sections (400 μm) containing the dorsal hippocampus were cut with a vibratome (Vibratome 1000 Plus), transferred to a holding chamber and incubated at room temperature for at least 60 min prior to recording. One slice was then transferred to a liquid–air interface chamber (Fine Science Tools, Inc., Foster City, CA, USA) and suspended on a nylon net at the liquid–air interface in a bath of continuously dripping oxygenated ACSF (2–2.5 ml/min). Humidified carbogen was passed along the upper surface of the slice, and bath temperature was set at 30 $\pm$ 1°C.

Electrophysiological Recordings

Patch-Clamp Recording from Hippocampal Slices Prepared from Young Mice

Patch-clamp whole-cell recording was performed at 32 $\pm$ 1°C using a patch-clamp amplifier (Multiclamp 700A; Axon Instruments, Foster City, CA, USA) under infrared-DIC (differential interference contrast) microscopy (Zeiss Axionskop2 FS Plus, Thornwood, NY, USA). Temperature of the recording chamber was set to 32° C and maintained by an automatic temperature controller (TC-324B; Warner Ins. Hamden, CT, USA). Data acqui-

sition and analysis were performed using a digitizer (DigiData 1322A; Axon Instruments) with pClamp 9.2 analysis software (Axon Instruments) and Mini Analysis 6 (Synaptosoft, Inc., Decatur, GA, USA). Signals were filtered at 2 KHz and sampled at 10 KHz. For presynaptic stimulation, a bipolar tungsten stimulation electrode (WPI, Sarasota, FL, USA) was placed approximately 150–200 μm rostral to the recording electrode, and stimulation was delivered through a stimulator (Model 2100 AM stimulator, Carlsborg, WA, USA). Stimulus intensity was set to a level which induced 50% maximal response. The interval of paired-pulse stimulation was 50 mseconds. To induce synaptic long-term potentiation (LTP), high frequency, tetanic stimulation (100 Hz, 1 second × 3 at 20-second intervals) was delivered. To measure synaptic events, the neuron was voltage-clamped at −60 mV in the presence of a $GABA_A$ receptor antagonist picrotoxin (PTX, 100 μM) or ionotropic glutamate receptor antagonists (CNQX 20 μM and D-APV 50 μM) based on the monitor of spontaneous excitatory postsynaptic currents (sEPSCs) or inhibitory postsynaptic currents (sIPSCs). The whole-cell recording pipette (3–4 MΩ) was filled with a solution containing (in mM): 120 $CsCH_3SO_3$, 20 HEPES, 0.4 EGTA, 2.8 NaCl, 5 TEA-Cl, 2 $MgCl_2$, 2.5 MgATP, and 0.3 GTP (pH 7.2–7.4 with CsOH). All drugs were obtained from Tocris Cookson Inc. (Ballwin, MO, USA). Values are expressed as mean ± SEM. Statistical significance was assessed as $P < 0.05$ using Student's two-tailed *t*-tests.

Field Potential Recordings from Hippocampal Slices

Standard extracellular field potential recordings were performed in the stratum radiatum of the hippocampal CA1 region using borosilicate glass micropipettes pulled to a tip diameter of about 1 μm and filled with 2 M NaCl [38,39]. Evoked field excitatory postsynaptic potentials (fEPSPs) (recording electrode was placed underneath cell layer) or field population spikes (recording electrode was placed on cell layer) were recorded using an Axoclamp-2B amplifier (Axon Instruments, Inc., Union City, CA, USA). The Schaffer collaterals were stimulated with a custom bipolar platinum wire electrode (diameter 0.003″) connected to a Model 2100 AM Systems Isolated Pulse Stimulator (Carlsborg, WA, USA). Stimulus intensity was determined using input/output response curves and was set at 50% of the maximal response. LTP was induced by high-frequency tetanic stimulations (100 Hz, 1 second × 3 at 20-second intervals) and theta-burst stimulations (one or five trains) of the Schaffer collaterals following a stable 20-min baseline. fEPSPs were subsequently recorded for an additional 60 min at 0.033 Hz. Data were acquired through an Axon Digidata 1322 (Axon Instruments) interface board set to a sampling frequency of 10 kHz and controlled with pClamp 9.2 (Axon Instruments), filtered in Clampfit 9.2 (Axon Instruments) using an 8-pole Bessel filter and a 1 kHz low-pass filter, and stored on hard media for subsequent off-line analysis.

Data Analysis

Statistical comparisons using Student's *t*-test (independent or paired) or analysis of variance were performed with Origin 5.0 (Microcal Software, Inc., Northampton, MA, USA). *P*-values <0.05 were considered to be statistically significant.

Results

Basic Electrophysiological Properties of Hippocampal CA1 Pyramidal Neurons in Young MeCP2 A140V Mice

Initial experiments were designed to compare electrophysiological characteristics between MeCP2 A140V and WT mice. Patch-clamp whole-cell recording was performed in the pyramidal neurons of hippocampal slices. Results showed that under our experimental conditions, most recorded hippocampal pyramidal neurons did not show regularly spontaneous action potential (AP) firing in either A140V or WT mice. In 30 hippocampal pyramidal neurons (from 19 A140V mutant mice) tested, the resting membrane potential (RP) was −59.8 ± 1.8 mV, while in pyramidal neurons tested from 10 WT neurons (from six mice), RP was −64.0 ± 1.6 mV. The difference of the RPs between A140V and WT neurons was significant ($P < 0.05$, Figure 1Da). Injection of depolarizing currents (e.g., 30–50 pA) via recording electrode induced AP firing and showed that the frequency of AP firing in response to the same current injection (e.g., 50 pA) was significantly higher in A140V neurons (Figure 1B) than in WT neurons (Figure 1A). Input/output (I/O) relation curves derived from plots of spike numbers occurring as a function of injected, depolarizing currents (30, 40, 50 pA) showed that there was a significantly higher firing rate ($P < 0.05$) in response to 50 pA current injection in A140V neurons (n = 10 from six mice) than in the WT neurons (n = 8 from five mice) (Figure 1C). Further analysis of AP found that although there was no difference in AP amplitude between A140V (75.2 ± 2.7 mV, n = 24 from 18 mice; Figure 1Db) and WT neurons (79.0 ± 2.9 mV, n = 9 from seven mice, $P > 0.05$; Figure 1Db), the A140V neurons exhibited a wider AP duration and lower after hyperpolarization (AHP) compared to WT neurons (AP duration: A140V = 1.38 ± 0.06 mseconds, n = 24 from 18 mice; WT = 1.15 ± 0.04 mseconds, n = 9 from seven mice; $P < 0.05$, Figure 1Dc; AHP amplitude: A140V = −4.42 ±0.44 mV, n = 20 from 13 mice; WT = −9.73 ± 1.61, n = 7 from five mice; $P < 0.05$, Figure 1Dd).

To explore a possible role of A-type K^+ channels in these electrophysiological changes in A140V neurons, we compared the A-type voltage-gated K^+ channels in hippocampal CA1 pyramidal neurons in A140V and WT mice. The A-current was elicited using two types of prepulse protocols [40]. In the first protocol, a 500 mseconds prepulse from a holding potential of −60 mV to −100 mV was applied, then a series of depolarizing test voltage steps from −90 mV to −10 mV in 10 mV increments were applied (Figure S1Aa). In the second protocol, a 500 mseconds prepulse from a holding potential of −60 mV to −40 mV was given before various depolarizing test voltage steps from −90 mV to −10 mV in 10 mV increments were applied (Figure S1Ab). The A-current was obtained by subtracting currents in the second protocol from corresponding currents in the first protocol (Figure S1Aa–b). We measured peak amplitude of A-currents (indicated by vertical dashed line in Figure S1Aa–b) in both A140V and WT neurons. Results demonstrated that A140V neurons exhibited a significantly lower level of A-currents than WT neurons (Figure S1B). Together, these results suggest that the A140V point mutation results in a series of electrophysiological alterations in hippocam-

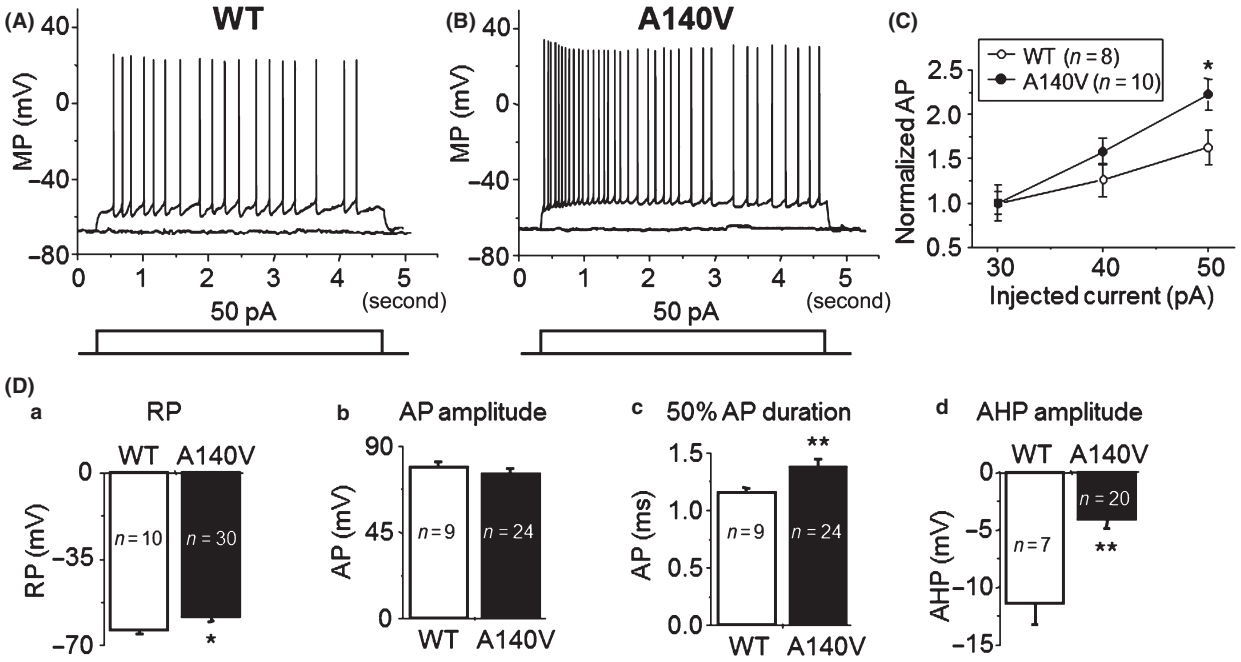

Figure 1 Electrophysiological comparisons between hippocampal neurons from A140V and WT mice. (**A**) Typical traces of AP firing of WT hippocampal neurons with and without injection of 50 nA current. Below the traces is the protocol of current injection. (**B**) Typical traces of AP firing of A140V hippocampal neurons using the same current injection protocol as A. Note, the RPs are the same in these two cases. (**C**) Input/output relation curves obtained from WT and A140V neurons. The AP numbers were normalized to the current injection with 30 pA. *means $P < 0.05$. (**D**) Statistical analysis demonstrates significant differences of RP and AP between A140V and WT hippocampal neurons. The number in each column indicates the neurons tested. The vertical bars represent ±MSE. *indicates $P < 0.05$, **indicates $P < 0.01$ in this and all following figures.

pal neurons and that reduced function of K^+ channels may underlie these abnormalities.

Comparison of GABAergic and Glutamatergic Synaptic Transmissions onto Hippocampal Pyramidal Neurons between Young A140V and WT Mice

In these experiments, we asked whether or not the A140V mutation altered inhibitory and/or excitatory neurotransmission. For analyses of inhibitory neurotransmission, we measured sIPSCs in the presence of 20 μM CNQX and 50 μM D-APV. For analysis of excitatory neurotransmission, we measured spontaneous excitatory postsynaptic currents (sEPSCs) in the presence of 100 μM picrotoxin (PTX) in the voltage-clamp mode. Figure 2 shows that A140V neurons had lower levels of sIPSC frequency (Aa and Ba) and amplitude compared to WT neurons (Ab and Bb). However, there was no significant difference of sEPSCs between A140V and WT neurons (C and D). These results suggest that the A140V mutation likely impairs GABAergic transmission onto pyramidal neurons in hippocampal slices.

Then, we further tested evoked EPSCs (eEPSC) and IPSCs (eIPSC) in both WT and A140V mutation mice. The eEPSC responses to presynaptic paired-pulse stimuli were measured at an interpulse interval of 50 mseconds [41] in the presence of the $GABA_A$ receptor antagonist PTX (100 μM) to ensure the elimination of stimulation-induced effects on inhibitory neurotransmission. As shown in supplemental Figure 2, the paired-pulse EPSC ratio (P2/P1; PPR) was significantly decreased in slices prepared from A140V mice (Figure S2A, red trace) relative to that from WT mice (Figure S2A, black trace). The values of EPSP paired-pulse facilitation (PPR) were 1.76 ± 0.08 (n = 6 from four mice) for WT and 1.47 ± 0.11 (n = 6 from four mice) for A140V mice ($P < 0.05$). These results suggest that there is an increase in the probability of evoked presynaptic glutamate release in the A140V hippocampal CA3-CA1 synapses.

As it is known that GABA-mediated inhibition suppresses induction of LTP at many excitatory synapses [42–45], we further compared paired-pulse inhibition of evoked IPSCs between WT and A140V mice. We examined evoked inhibitory postsynaptic currents (eIPSCs) under voltage-clamp conditions evoked by paired-pulse stimuli at an interpulse interval of 50 mseconds at a holding potential (V_H) of −60 mV in the presence of NBQX (10 μM) and D-APV (50 μM) to block glutamate receptor responses [46]. Stimulation intensity was gradually increased until threshold for production of IPSCs was reached, and then, we used double threshold intensity to reliably induce IPSCs. The results showed that there was no significant change in the ratio of P2/P1 between WT (Figure S2Ba, black trace) and A140V (Figure S2Ba, red trace) mice, suggesting that the probability of evoked presynaptic GABA release is not altered in A140V mice compared to WT mice.

Synaptic LTP in Young A140V and WT Mice

We have demonstrated abnormalities of synaptic function in young A140V mutant mice. The logical question is whether these

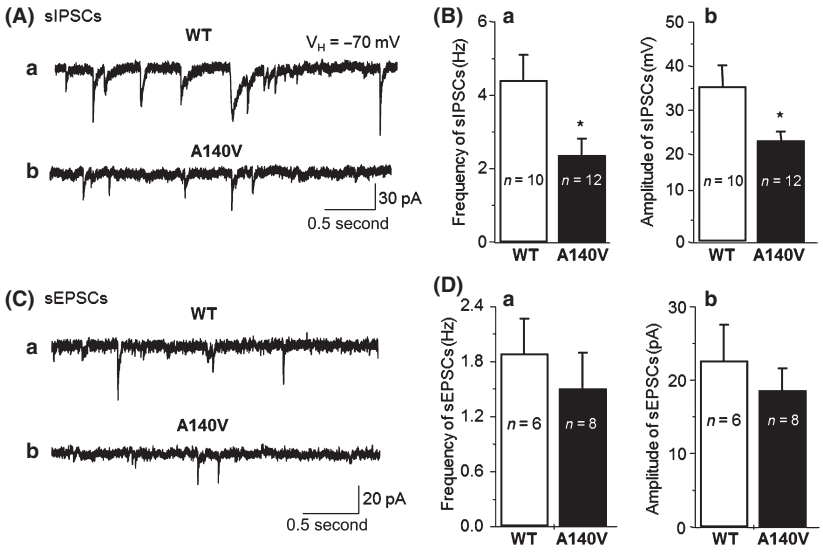

Figure 2 Spontaneous inhibitory postsynaptic currents (sIPSCs) and sEPSCs in A140 and WT hippocampal neurons. (**A**) Typical traces of sIPSCs of WT (**Aa**) and A140V (**Ab**) neurons. (**B**) Statistical analysis shows that A140V neurons have lower sIPSC frequency (**Ba**) and amplitude (**Bb**). (**C**) Typical traces of sEPSCs of WT (**Ca**) and A140V (**Cb**) neurons. (**D**) Analysis shows that A140V neurons have slightly lower sEPSC frequency (**Da**) and amplitude (**Db**) compared to WT neurons, but the difference is not statistically significant.

alterations in hippocampal electrophysiology and synaptic function affect synaptic plasticity, a cellular basis of animal learning and memory. To address this question, we examined hippocampal CA3-CA1 synaptic plasticity in young A140V mutant and WT mice. In these experiments, we measured hippocampal CA3-CA1 synaptic LTP in young (30- to-40-day-old) WT and A140V mutant mouse hippocampal slices (400 μm thickness) using field potential recording. LTP was induced by high-frequency (HF) stimulation of the Schaffer collaterals (three 1 second bursts at 100 Hz with 20-second interburst intervals). Baseline fEPSPs were recorded every 30 seconds for 10–20 min. Stimulation intensity was set to elicit fEPSPs with slopes that were 50% of the maximal response. If the variation in baseline fEPSP slopes was $< \pm 10\%$, tetanic stimulation was delivered and fEPSPs were recorded for an additional 30 min (Figure 3A,B). Results showed that there was no significant difference in HF tetanic stimulation-induced LTP between WT and A140V mutant mice (Figure 3C). These results suggest that there is no significant impairment of hippocampal CA3-CA1 synaptic plasticity in young A140V mutant mice.

Comparison of Neural Excitability between Adult A140V and WT Mice

Data presented thus far in young A140V mutant mice showed some electrophysiological abnormalities, but we did not find significant impairment of hippocampal CA3-CA1 synaptic plasticity (LTP). We therefore designed a series experiments to examine neural excitability, synaptic short-term and long-term plasticity in adult (11- to 13-month-old) A140V and WT mice. To test neural excitability, the Schaffer collateral pathway was stimulated at progressively higher intensities (from 1 to 8 V at intervals of 30 seconds), and the amplitudes of the field population spikes (PS, recording electrode was place at cell layer) were plotted against stimulation intensities to create input/output response curves. As showed in Figure 4A, the PS amplitudes were larger in A140V slices compared to WT slices when stimulation intensities were 3–8 V, respectively. After linear fitting analysis (Figure 4B), the linear slope for WT group was -0.34 ± 0.01 mV/mseconds (n = 31 from 21 mice), while that for A140V group was -0.49 ± 0.02 (n = 31 from 19 mice, $P < 0.05$). These results suggest that adult A140V mice exhibit higher excitability in hippocampal neurons compared to age-matched WT mice, which is consistent with the finding in young mice.

Comparison of Paired-Pulse Responses between Adult A140V and WT Mice

During paired-pulse stimulation, two stimuli are applied within 50–200 mseconds of each other. In response to the second stimulus, there is a transient increase in the fEPSP called paired-pulse facilitation (PPF). When the interpulse intervals are shorter than 30 mseconds, there is usually a transient reduction in the second response (paired-pulse depression, PPD) [47]. We examined paired-pulse responses of field PS using interpulse intervals of 15, 30, 50, 100, and 150 mseconds in WT and A140V mice. The typical traces demonstrated a PPD (15 and 30 mseconds interval) but little PPF (>50 mseconds) in A140A slices as shown in Figure 5A (black traces are first response and gray traces are second response). Figure 5B shows typical traces from WT slices, in which, 50 mseconds or longer stimulation interval (50 mseconds) enhanced PPF (A140V, n = 21 from 14 mice vs. WT, n = 18 from 11 mice: $P < 0.05$, Figure 5C). Together, these results suggest an impaired short-term synaptic plasticity in A140V mice.

Comparison of Field Population Spike (PS) LTP in Adult WT and A140V Hippocampal Slices

In these experiments, we compared the response to different forms of tetanic stimulation-induced field PS LTP in WT and A140V slices (the recording electrode was placed at the cell layer). First, the field PS LTP was induced by HF stimulation of the Schaffer collaterals (three 1 second bursts at 100 Hz with 20-second interburst intervals). Stimulation intensity was set to elicit field PS with slopes that were 50% of the maximal response. Baseline field

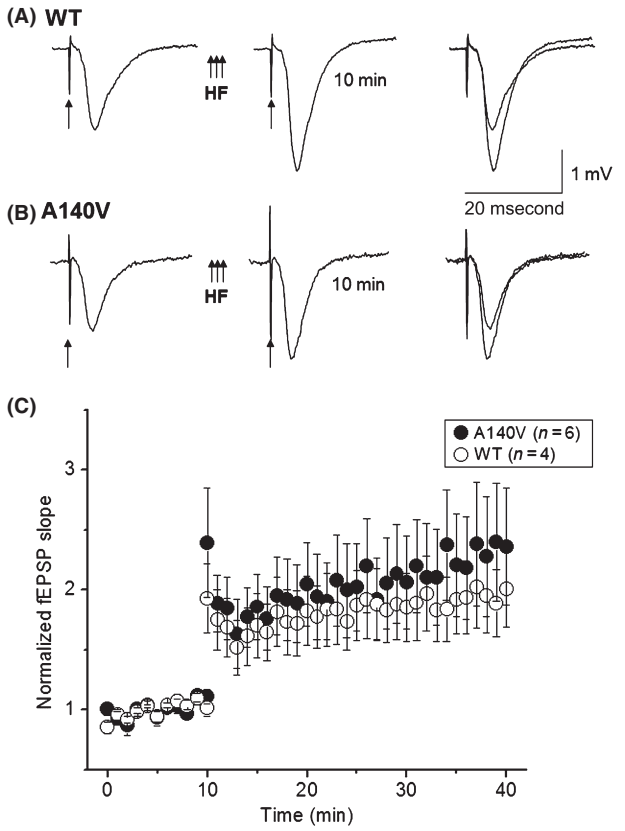

Figure 3 Comparison of high-frequency (HF) long-term potentiation (LTP) in young WT and A140V mutant mice. Typical field excitatory postsynaptic potentials (fEPSP)s from WT (**A**) and A140V slices (**B**) (**C**) compared to WT (black, n = 7) responses, A140V slices (red, n = 6) did not show significant impairment of LTP.

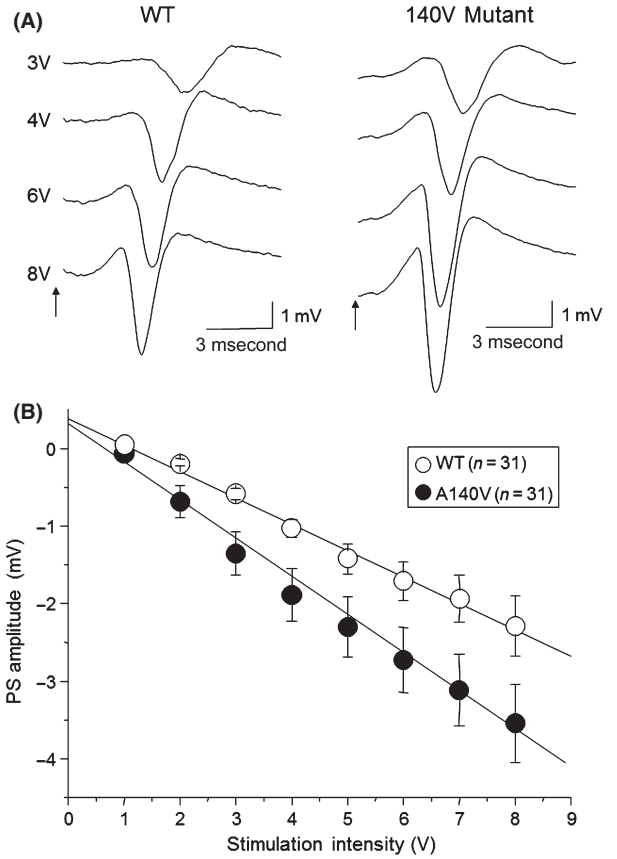

Figure 4 Comparison of input/output relationship curves in adult WT and A140V mice. Hippocampal slices were used to generate input/output response curves. (**A**) Representative field population spike (PS) traces of different stimulation intensities in WT (left panel) and A140V mutant mice (right panel). (**B**) The amplitudes of field PS are illustrated for stimulation intensities ranging from 1 to 8 V. The slope of input/output curve (determined using linear regression) was significantly increased in A140V mice compared to WT mice.

PSs were recorded every 30 seconds for 20 min. If the variation in baseline field PS slopes was < ±10%, HF tetanic stimuli were delivered and field PSs were recorded for an additional 60 min. Results demonstrated that there was no significant difference of HF-induced LTP between adult WT (n = 9 from six mice) and A140V mice (n = 9 from seven mice, $P > 0.05$, Figure 6A).

Then, we compared theta-burst stimulation (TBS)-induced field PS LTP between adult WT and A140V mice. The TBS was set up as five trains (five pulses at 100 Hz) with an interval of 200 mseconds (5 Hz) for 2 seconds, and the same stimuli were repeated three times with an interval of 20 seconds. As shown in Figure 6B, TBS ×5 stimulation induced a lower level of LTP in A140V mice (n = 6 from five mice) compared to WT mice, but the difference was not significant (n = 6 from four mice, $P > 0.05$). Next, we delivered the weaker stimuli (TBS with one pulse), which is similar to weak presynaptic stimulation (WPS) [41]. By using this weaker stimulation, A140V slice (n = 12 from nine mice) showed a significant impairment of LTP level compared to WT slices (n = 9 from eight mice, $P < 0.05$; Figure 6C). These results suggest that the alterations of hippocampal CA3-CA1 synaptic plasticity in A140V mice are likely mild, which can only be detected at weak stimulation.

Finally, we compared TBS (one or five trains) tetanic stimuli-induced field excitatory postsynaptic potential (fEPSP) LTP in WT and A140V slices. The recording electrode was placed below the cell layer to obtain fEPSPs. Baseline fEPSPs were recorded every 30 seconds for 20 min. Stimulation intensity was set to elicit fEPSPs with slopes that were 50% of the maximal response. If the variation in baseline fEPSP slopes was < ±10%, tetanic stimulation was delivered and fEPSPs were recorded for an additional 60 min (Figure S3A). In the WT group (n = 9 from six mice), TBS ×5 stimulation of the Schaffer collaterals resulted in an increase in the fEPSP slope (from baseline 1.0 increased to 1.72 ± 0.07 at 1 min and 1.51 ± 0.12 at 60 min after tetanic stimulation). In the A140V mutant group (n = 6 from four mice), TBS ×5 stimulation induced an increase in fEPSP slope (1.52 ± 0.17 and 1.49 ± 0.11 after TBS ×5 1 and 60 min), which was not significantly different compared to WT LTP ($P > 0.05$). In addition, TBS ×1 tetanic stimulation did not induce typical fEPSP LTP in either WT or A140V mutant mice (Figure S3B). These results suggest that A140V mutant mice exhibit a quite mild impairment of hippocampal CA3-CA1 synaptic LTP.

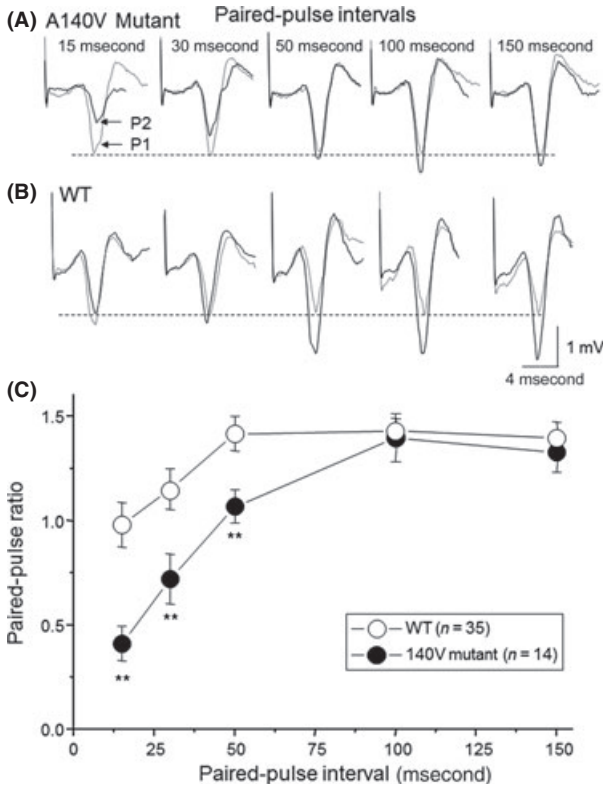

Figure 5 Paired-pulse responses in WT and A140V mice. (**A**) Representative typical traces of paired-pulse response induced by presenting two stimuli with different interpulse intervals (IPI) of 15, 30, 50, 100, and 150 mseconds in A140V mutant (**A**) and WT mice (**B**). The gray traces represented as first pulse-induced response, while black traces represented as second pulse-induced response (**C**) Paired-pulse ratios (P2/P1) for IPI of 15, 30, 50, 100, and 150 mseconds are illustrated. In these experiments, the PS amplitudes were measured.

Discussion

In our current studies, we have confirmed the presence of hippocampal electrophysiological abnormalities in the male MeCP2 A140V mutant mice. The basic electrophysiological properties of neurons from the A140V mice were found to be different from those of WT mice and included more positive resting membrane potentials, a shift of input/output relationship curve to the left, wider action potential duration, and decreased after hyperpolarization amplitude. Reduced spontaneous neuronal firing rates have also been previously noted in MeCP2-null mouse layer 5 cortical neurons [27], but in our study, we rarely saw regularly spontaneous firing of hippocampal CA1 pyramidal neurons. The change in resting membrane potential and longer action potential duration identified in neurons from the A140V mice could result from abnormal potassium channel function, and indeed, we identified low levels of functional potassium channels that affected the A-type currents associated with rapidly inactivating potassium channels. The low levels of these channels likely resulted in a slower inactivation process which increased the action potential duration seen in our experiments.

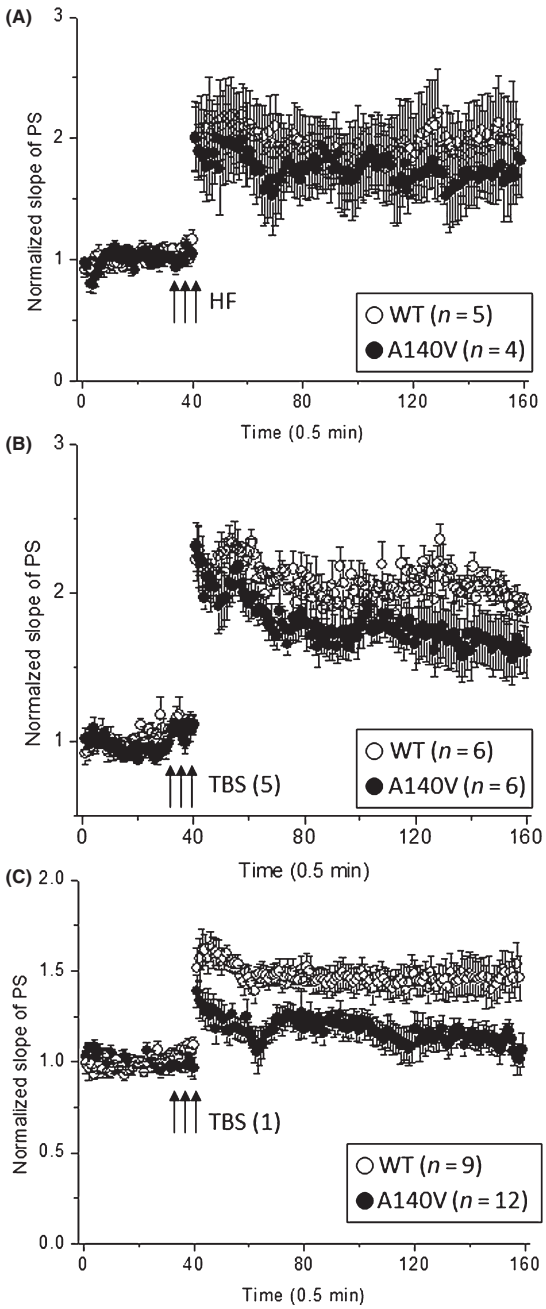

Figure 6 Different types of tetanic stimuli induces field PS long-term potentiation (LTP) in WT and A140V mice. Recoding electrode was placed at the cell layer to obtain field PSs. (**A**) Summary of results from high-frequency (HF)-induced field PS LTP in WT and A140V mutant mice. Statistical analysis showed that after HF stimuli 1 min and 60 min, the LTP levels are not significantly different between WT and AV140V mice. (**B**) Summary of results from theta-burst stimulation (TBS) ×5-induced field PS LTP in WT and A140V mutant mice. Statistical analysis showed that after TBS ×5 stimuli 1 min and 60 min, the LTP levels are not significantly different between WT and AV140V mice. (**C**) Summary of results from TBS ×1-induced field PS LTP in WT and A140V mutant mice. Statistical analysis showed that after TBS ×1 stimuli 1 min and 60 min, the LTP level in A140V mutant mice was significantly impaired compared to that in WT mice.

In A140V mice, there is a significant decrease in the frequency and amplitude of sIPSC, implying an abnormality of the spontaneous release of presynaptic GABA transmitter. The role of aberrant GABA signaling in the RTT phenotype has been shown in a mouse model, in which MeCP2 was lacking in GABAergic neurons [48]. These mice displayed abnormalities of learning and motor function as well as other features consistent with RTT or autism phenotypes. Experiments previously performed on female MeCP2-null mice have also found that the frequency of spontaneous IPSP-based rhythmic activity is reduced [33]. Together, these results indicate that MeCP2 could be involved in the regulation of basal inhibitory signals in the brain, which may present as neuronal hyperexcitability.

Neuronal excitability in the hippocampus was found to be significantly increased in both young and older A140V mice as evidenced by the results of input/output experiments which showed increased action potential firing in young mice and increased amplitude of population spikes in adult mice. Hyperexcitability of neurons in the hippocampus has also been described in a study of adult female heterozygous MeCP2-null mice [33]. A second study in male hemizygous MeCP2-null mice identified this same phenomenon using voltage-sensitive dye imaging. The male mouse study also found that both the CA1 and CA3 neurons in MeCP2-null mice are hyperactive and that severing CA3 contact with CA1 results in normalization of CA1 activity [49]. The finding of increased neuronal excitability in the A140V mice parallels that seen in MeCP2-null mice [33,49] and implies that the A140V point mutation is sufficient to disrupt a function that is also disrupted when the full MeCP2 gene is lost. The present results demonstrated that under resting conditions, there was a decrease in sIPSC frequency and amplitude, suggesting a reduction in GABAergic transmission, which might lead to an impaired inhibition during the resting state.

The paired-pulse facilitation and inhibition fEPSP experiments performed on neurons from adult mice suggested an impaired short-term plasticity in the A140V mice. This deficit is implied by both a strong paired-pulse depression following pulses at intervals shorter than 30 seconds as well as by enhanced paired-pulse facilitation at pulse intervals of 50 seconds. This may suggest an impairment of feedback inhibition by GABAergic neurons. In contrast to this, an fEPSP paired-pulse study of MeCP2-null mice found a decrease in paired-pulse facilitation at stimulus intervals of 50 and 100 mseconds [31]. This suggests that in our A140V mutant model alterations (impairments) of GABAergic transmission, rather than glutamatergic transmission, likely play an important role in the functional changes of this animal model. Paired-pulse eEPSC experiments carried out in neurons from young A140V mice using the slice patch-clamp whole-cell recording found a decreased paired-pulse ratio, which may indicate an increase in presynaptic glutamate release probability that could be related to the observed neuronal hyperexcitability.

Long-term plasticity was also tested in both young and adult A140V mice. High-frequency tetanic stimulation of neurons from young mice found no significant difference in the generation of LTP in A140V versus WT neurons. When field population spike LTP was tested in adult mice using the high-frequency stimulation protocol, there was again no significant difference between A140V and WT neurons. However, when theta-burst stimulation protocols were used in place of high-frequency protocols, significant differences were found in LTP which may reflect mild abnormalities of hippocampal CA3-CA1. Measurements of hippocampal LTP in symptomatic MeCP2-null mice previously showed decreased LTP using both high frequency and theta-burst stimulation protocols [31]. Likewise, LTP deficits were identified in both hippocampal and cortical neurons from MeCP2 308/Y mutant mice [30]. The finding of potential LTP deficits in A140V mice by only the theta-burst protocol implies that neurons from A140V mice are demonstrating a milder deficit than that seen in the null or 308/Y mice, which correlates with overall symptom severity which is also milder in A140V mice.

Conclusions

MeCP2 A140V mice exhibit various electrophysiological abnormalities that are generally consistent with those seen in other MeCP2 mutant mouse models. This suggests that this point mutation is sufficient to disrupt neuronal signaling, although in a less prominent manner than that seen in null mice. It also provides information that may be useful in determining the functional cause of the cognitive and neurological symptoms seen in patients, particularly males, who carry the MeCP2 A140V mutation.

Acknowledgments

This work was supported by Arizona Biomedical Research Commission (ABRC) and Barrow Neurological Foundation (BNF) grants. The authors thank Harrison Stratton and Key-min Kim for their assistance with data analysis.

Conflict of Interest

The authors declare no conflict of interest.

References

1. Bird A. The methyl-CpG-binding protein MeCP2 and neurological disease. *Biochem Soc Trans* 2008;**36**(Pt 4):575–583.
2. Chahrour M, Jung SY, Shaw C, et al. MeCP2, a key contributor to neurological disease, activates and represses transcription. *Science* 2008;**320**:1224–1229.
3. Bienvenu T, Chelly J. Molecular genetics of Rett syndrome: When DNA methylation goes unrecognized. *Nat Rev Genet* 2006;**7**:415–426.
4. Chadwick LH, Wade PA. MeCP2 in Rett syndrome: Transcriptional repressor or chromatin architectural protein? *Curr Opin Genet Dev* 2007;**17**:121–125.
5. Georgel PT, Horowitz-Scherer RA, Adkins N, Woodcock CL, Wade PA, Hansen JC. Chromatin compaction by human MeCP2. Assembly of novel secondary chromatin structures in the absence of DNA methylation. *J Biol Chem* 2003;**278**:32181–32188.
6. Nan X, Campoy FJ, Bird A. MeCP2 is a transcriptional repressor with abundant binding sites in genomic chromatin. *Cell* 1997;**88**:471–481.
7. Skene PJ, Illingworth RS, Webb S, et al. Neuronal MeCP2 is expressed at near histone-octamer levels and globally alters the chromatin state. *Mol Cell* 2010;**37**:457–468.
8. Amir RE, Van den Veyver IB, Wan M, Tran CQ, Francke U, Zoghbi HY. Rett syndrome is caused by mutations in X-linked MECP2, encoding methyl-CpG-binding protein 2. *Nat Genet* 1999;**23**:185–188.
9. Chahrour M, Zoghbi HY. The story of Rett syndrome: From clinic to neurobiology. *Neuron* 2007;**56**:422–437.

10. Hagberg B. Rett's syndrome: Prevalence and impact on progressive severe mental retardation in girls. *Acta Paediatr Scand* 1985;**74**:405–408.
11. Hagberg B, Aicardi J, Dias K, Ramos O. A progressive syndrome of autism, dementia, ataxia, and loss of purposeful hand use in girls: Rett's syndrome: Report of 35 cases. *Ann Neurol* 1983;**14**:471–479.
12. Neul JL, Kaufmann WE, Glaze DG, et al. Rett syndrome: Revised diagnostic criteria and nomenclature. *Ann Neurol* 2010;**68**:944–950.
13. Neul JL, Zoghbi HY. Rett syndrome: A prototypical neurodevelopmental disorder. *Neuroscientist* 2004;**10**:118–128.
14. Kankirawatana P, Leonard H, Ellaway C, et al. Early progressive encephalopathy in boys MECP2 mutations. *Neurology* 2006;**67**:164–166.
15. Armstrong D, Dunn JK, Antalffy B, Trivedi R. Selective dendritic alterations in the cortex of Rett syndrome. *J Neuropathol Exp Neurol* 1995;**54**:195–201.
16. Bauman ML, Kemper TL, Arin DM. Pervasive neuroanatomic abnormalities of the brain in three cases of Rett's syndrome. *Neurology* 1995;**45**:1581–1586.
17. Belichenko PV, Oldfors A, Hagberg B, Dahlstrom A. Rett syndrome: 3-D confocal microscopy of cortical pyramidal dendrites and afferents. *NeuroReport* 1994;**5**:1509–1513.
18. Chapleau CA, Calfa GD, Lane MC, et al. Dendritic spine pathologies in hippocampal pyramidal neurons from Rett syndrome brain and after expression of Rett-associated MECP2 mutations. *Neurobiol Dis* 2009;**35**:219–233.
19. Ramocki MB, Tavyev YJ, Peters SU. The MECP2 duplication syndrome. *Am J Med Genet A* 2010;**152A**:1079–1088.
20. Moog U, Smeets EE, van Roozendaal KE, et al. Neurodevelopmental disorders in males related to the gene causing Rett syndrome in females (MECP2). *Eur J Paediatr Neurol* 2003;**7**:5–12.
21. Dotti MT, Orrico A, De Stefano N, et al. A Rett syndrome MECP2 mutation that causes mental retardation in men. *Neurology* 2002;**58**:226–230.
22. Klauck SM, Lindsay S, Beyer KS, Splitt M, Burn J, Poustka A. A mutation hot spot for nonspecific X-linked mental retardation in the MECP2 gene causes the PPM-X syndrome. *Am J Hum Genet* 2002;**70**:1034–1037.
23. Kudo S, Nomura Y, Segawa M, et al. Functional characterisation of MeCP2 mutations found in male patients with X linked mental retardation. *J Med Genet* 2002;**39**:132–136.
24. Orrico A, Lam C, Galli L, et al. MECP2 mutation in male patients with non-specific X-linked mental retardation. *FEBS Lett* 2000;**481**:285–288.
25. Winnepenninckx B, Errijgers V, Hayez-Delatte F, Reyniers E, Frank Kooy R. Identification of a family with nonspecific mental retardation (MRX79) with the A140V mutation in the MECP2 gene: Is there a need for routine screening? *Hum Mutat* 2002;**20**:249–252.
26. Jentarra GM, Olfers SL, Rice SG, et al. Abnormalities of cell packing density and dendritic complexity in the MeCP2 A140V mouse model of Rett syndrome/X-linked mental retardation. *BMC Neurosci* 2010;**11**:19.
27. Dani VS, Chang Q, Maffei A, Turrigiano GG, Jaenisch R, Nelson SB. Reduced cortical activity due to a shift in the balance between excitation and inhibition in a mouse model of Rett syndrome. *Proc Natl Acad Sci U S A* 2005;**102**:12560–12565.
28. Dani VS, Nelson SB. Intact long-term potentiation but reduced connectivity between neocortical layer 5 pyramidal neurons in a mouse model of Rett syndrome. *J Neurosci* 2009;**29**:11263–11270.
29. Lonetti G, Angelucci A, Morando L, Boggio EM, Giustetto M, Pizzorusso T. Early environmental enrichment moderates the behavioral and synaptic phenotype of MeCP2 null mice. *Biol Psychiatry* 2010;**67**:657–665.
30. Moretti P, Levenson JM, Battaglia F, et al. Learning and memory and synaptic plasticity are impaired in a mouse model of Rett syndrome. *J Neurosci* 2006;**26**:319–327.
31. Asaka Y, Jugloff DG, Zhang L, Eubanks JH, Fitzsimonds RM. Hippocampal synaptic plasticity is impaired in the Mecp2-null mouse model of Rett syndrome. *Neurobiol Dis* 2006;**21**:217–227.
32. Chao HT, Zoghbi HY, Rosenmund C. MeCP2 controls excitatory synaptic strength by regulating glutamatergic synapse number. *Neuron* 2007;**56**:58–65.
33. Zhang L, He J, Jugloff DG, Eubanks JH. The MeCP2-null mouse hippocampus displays altered basal inhibitory rhythms and is prone to hyperexcitability. *Hippocampus* 2008;**18**:294–309.
34. Zhang ZW, Zak JD, Liu H. MeCP2 is required for normal development of GABAergic circuits in the thalamus. *J Neurophysiol* 2010;**103**:2470–2481.
35. Medrihan L, Tantalaki E, Aramuni G, et al. Early defects of GABAergic synapses in the brain stem of a MeCP2 mouse model of Rett syndrome. *J Neurophysiol* 2008;**99**:112–121.
36. Taneja P, Ogier M, Brooks-Harris G, Schmid DA, Katz DM, Nelson SB. Pathophysiology of locus ceruleus neurons in a mouse model of Rett syndrome. *J Neurosci* 2009;**29**:12187–12195.
37. Ye JH, Zhang J, Xiao C, Kong JQ. Patch-clamp studies in the CNS illustrate a simple new method for obtaining viable neurons in rat brain slices: Glycerol replacement of NaCl protects CNS neurons. *J Neurosci Methods* 2006;**158**:251–259.
38. Wu J, Fisher RS. Hyperthermic spreading depressions in the immature rat hippocampal slice. *J Neurophysiol* 2000;**84**:1355–1360.
39. Song C, Murray TA, Kimura R, et al. Role of alpha7-nicotinic acetylcholine receptors in tetanic stimulation-induced gamma oscillations in rat hippocampal slices. *Neuropharmacology* 2005;**48**:869–880.
40. Koyama S, Appel SB. A-type K^+ current of dopamine and GABA neurons in the ventral tegmental area. *J Neurophysiol* 2006;**96**:544–554.
41. Pu L, Liu QS, Poo MM. BDNF-dependent synaptic sensitization in midbrain dopamine neurons after cocaine withdrawal. *Nat Neurosci* 2006;**9**:605–607.
42. Meredith RM, Floyer-Lea AM, Paulsen O. Maturation of long-term potentiation induction rules in rodent hippocampus: Role of GABAergic inhibition. *J Neurosci* 2003;**23**:11142–11146.
43. Bissiere S, Humeau Y, Luthi A. Dopamine gates LTP induction in lateral amygdala by suppressing feedforward inhibition. *Nat Neurosci* 2003;**6**:587–592.
44. Huang ZJ, Kirkwood A, Pizzorusso T, et al. BDNF regulates the maturation of inhibition and the critical period of plasticity in mouse visual cortex. *Cell* 1999;**98**:739–755.
45. Wigstrom H, Gustafsson B. Facilitated induction of hippocampal long-lasting potentiation during blockade of inhibition. *Nature* 1983;**301**:603–604.
46. Gao M, Jin Y, Yang K, Zhang D, Lukas RJ, Wu J. Mechanisms involved in systemic nicotine-induced glutamatergic synaptic plasticity on dopamine neurons in the ventral tegmental area. *J Neurosci* 2010;**30**:13814–13825.
47. Zucker RS, Regehr WG. Short-term synaptic plasticity. *Annu Rev Physiol* 2002;**64**:355–405.
48. Chao HT, Chen H, Samaco RC, et al. Dysfunction in GABA signalling mediates autism-like stereotypies and Rett syndrome phenotypes. *Nature* 2010;**468**:263–269.
49. Calfa G, Hablitz JJ, Pozzo-Miller L. Network hyperexcitability in hippocampal slices from Mecp2 mutant mice revealed by voltage-sensitive dye imaging. *J Neurophysiol* 2011;**105**:1768–1784.

Supporting Information

The following supplementary material is available for this article:

Figure S1. A140V neurons express lower level of functional K^+ (A-type) channels.

Figure S2. Comparison of paired-pulse ratio (PPR) in WT and A140V mutant mice.

Figure S3. Field EPSP LTP in WT and A140V mutant mice.

